# Large extracellular vesicles derived from LPS-preconditioned cardiomyocytes alleviate myocarditis via mediating macrophage polarization and modulating p38 MAPK pathway

Yanjie Jiang[1,2,3†], Yingnan You[1†], Yaxue Xie[1,3], Shan Zhou[4], Mengjie Ma[4] and Bo Han[1,4*]

[1]Department of Pediatric Cardiology, Shandong Provincial Hospital Affiliated to Shandong First Medical University, Jinan, Shandong, China, [2]Department of Pediatrics, The Affiliated Taian City Central Hospital of Qingdao University, Tai'an, Shandong, China, [3]School of Medicine, Cheeloo College of Medicine, Shandong University, Jinan, Shandong, China, [4]Shandong First Medical University & Shandong Academy of Medical Sciences, Jinan, Shandong, China

**Introduction:** Myocarditis is an inflammatory injury to the myocardium characterized by disrupted intercellular communication, involving macrophages and cardiomyocytes as key players. However, the interactions between macrophages and cardiomyocytes during myocarditis remain inadequately explored. Emerging evidence indicated that extracellular vesicles (EVs) play a crucial role in intercellular communication.

**Methods:** In our study, LPS- or PBS-preconditioned cardiomyocytes derived large EVs (C-lEV$_{LPS}$/C-lEV$_{PBS}$) were isolated. qPCR, ROS and flow cytometry assays were employed to evaluate their impact on macrophages and in the in vivo experiments, C-lEV$_{LPS}$ was administered to mice with viral myocarditis. Cardiac function was assessed through echocardiography and cTnT levels, while inflammatory responses were analyzed via histopathological examination and cytokine profiling. Then mechanistic investigations were performed using integrated transcriptomic and proteomic profiling to characterize EV-mediated regulatory networks. Statistical analyses were performed using Student's t-test or ANOVA, with significance set at $p < 0.05$.

**Results:** We demonstrated C-lEV$_{LPS}$ exhibited anti-inflammatory effects on macrophages and alleviated cardiac inflammation and dysfunction in a mouse model of CVB3-induced myocarditis. Additionally, C-lEV$_{LPS}$ facilitated macrophage polarization toward the M2-like phenotype and inhibits M1 polarization, both in vitro and in vivo. Notably, compared to C-lEV$_{PBS}$, C-lEV$_{LPS}$ was enriched in the phosphatase 2 scaffold subunit alpha protein (PP2AA), which can recruit other subunits to form the PP2A complex, ultimately leading to the dephosphorylates of p38.

**Discussion:** This study highlights the effect of C-lEV$_{LPS}$ in myocarditis and uncovers the potential mechanism that modulates macrophage polarization by delivering PP2AA from cardiomyocytes to macrophages and regulating the p38 MAPK pathway. These findings provide a promising therapeutic strategy for myocarditis.

# 1 Introduction

Myocarditis, an inflammation of the heart muscle, presents a range of symptoms from mild fatigue and chest discomfort to severe complications such as arrhythmias, heart failure, cardiogenic shock, and sudden death (1, 2). The etiology of myocarditis is multifactorial, with common infectious agents including bacteria, viruses, fungi, and parasites. In developed countries, viral infections (such as Coxsackie virus B3 and adenovirus) are the most prevalent causes (1); whereas in tropical and subtropical regions, parasitic infections such as Chagas disease, toxoplasmosis, and schistosomiasis contribute significantly to the incidence of myocarditis (3). These pathogens can induce myocardial inflammation through direct invasion or immune-mediated mechanisms. Due to the incomplete understanding of myocarditis pathogenesis, specific treatment strategies are currently unavailable (1, 2).

Cardiomyocytes, the primary cellular components of the heart, are targeted during myocarditis by pathogens like viruses, leading to their replication within the host cells (1, 2, 4, 5). This results in direct damage characterized by swelling, apoptosis, and necrosis (4). Additionally, macrophages—the main immune cells in the heart (1, 5, 6)—accumulate at injury sites during myocarditis and exhibit significant phenotypic plasticity (6, 7). They are generally classified into M1 and M2 macrophages, where M1 macrophages enter injury sites and secrete pro-inflammatory cytokines that block tissue repair, while M2 macrophages aid in later healing stages by eliminating pathogens and encouraging the repair of inflammatory sites (8–10). Given the dynamic and heterogeneous nature of macrophages, targeting macrophage heterogeneity may offer new therapeutic avenues for myocarditis.

Communication between macrophages and cardiomyocytes usually occurs via direct contact, paracrine factors, or extracellular vesicles (EVs) (11). EVs are now recognized as critical modulators in both physiological and pathological processes, especially in contexts such as cardiovascular diseases (12–17). Notably, EVs serve as key mediators by transferring cellular substances like miRNA and proteins (18, 19). For instance, hypoxic cardiomyocytes release small EVs rich in TNF-α (20), while exosomes originating from M2 macrophages containing miRNA-148a and miRNA-378a-3p mitigate cardiomyocyte apoptosis and

pyroptosis following cardiac injury (19, 21). In the context of heart failure and myocardial infarction, EVs play crucial roles in cardiac repair, especially when triggered by cell therapy (22–24).

According to the MISEV 2023 recommendations, EVs are classified into small EVs (sEVs) and large EVs (lEVs, also referred to as microvesicles) based on size (25). Although sEVs might generally refer to EVs <200 nm in diameter and lEVs typically ranging from 150 nm to over 1,000 nm, there is no strict consensus on upper and lower size cut-offs (25, 26). And it has become clear that many separation methods, such as dUC, yield EV subpopulations with overlapping size distributions (25). Critically, compared with sEVs, lEVs carry unique bioactive molecules, such as specific protein signatures (27–29) and potentially distinct sets of miRNAs (30). These cargo molecules often fulfilling roles that differ from those attributed to sEVs (29), contributing significantly to processes like immunomodulation (31, 32) and tissue repair (9), Meanwhile, their larger size confers greater cargo capacity, enabling them to transport complex molecular or larger volumes of bioactive cargo for enhanced functional effects upon fusion with recipient cells (33) and larger membrane area enhancing their fusion ability with recipient cells (34). However, in myocarditis—an immune-mediated myocardial injury—the signaling functions and pathological regulatory mechanisms of EVs, particularly cardiomyocyte-derived lEVs (C-lEVs) with unique large cargo transport capacity, remain significantly understudied. Urgent multi-dimensional investigations are needed to uncover their potential value, thus offering new opportunities for the accurate diagnosis and targeted therapy of myocarditis.

This research investigated the impact of C-lEVs on myocarditis, focusing on the interaction between cardiomyocytes and macrophages. In our study, lipopolysaccharide (LPS) was used solely as an *in vitro* tool to simulate the inflammatory environment experienced by cardiomyocytes during infection or injury. The purpose was to dissect the molecular composition and function of C-lEVs secreted under defined stress conditions. Our findings revealed that lEVs derived from LPS-preconditioned cardiomyocytes (C-lEV$_{LPS}$) regulated macrophage polarization by altering M1/M2 macrophage marker expression and suppressing inflammatory cytokine production. Further investigation demonstrated that C-lEV$_{LPS}$ influenced macrophage polarization by interacting with the p38 MAPK pathway. Proteomic analysis

showed that C-lEV$_{LPS}$ delivers PP2AA to macrophages, thereby modulating the p38 MAPK pathway. Essentially, this research specifically looks into the involvement of C-lEVs in myocarditis, providing new insights into its pathogenesis and potential therapeutic approaches.

# 2 Materials and methods

## 2.1 Cell culture

The cardiomyocyte cell line H9C2, murine macrophage cell line RAW264.7, and human laryngeal squamous cell carcinoma Hep2 cells were purchased from Yanyi Biotech Co., Ltd. (Shandong, China). Cells were maintained in high-glucose DMEM supplemented with 10% fetal bovine serum and 1% penicillin-streptomycin (Solarbio, Shanghai, China) under conditions of 37 °C and 5% $CO_2$. H9C2 cells were starved for 12 hours and then exposed to 1.5 µg/mL LPS for 24 hours, while RAW264.7 cells received a 12-hour treatment with 1 µg/mL LPS to stimulate polarization. Following this, the therapeutic impact of C-lEVs was examined by introducing $1 \times 10^7$ C-lEVs particles to the culture medium. 100 nM Anisomycin(AM, MCE, #22862-76-6) was introduced into the culture medium to stimulate the MAPK signaling pathway.

## 2.2 Isolation and characterization of C-lEVs

The culture medium of H9C2 cardiomyocytes treated with PBS or LPS was collected, and the C-lEVs were obtained by differential centrifugation as previous described (9). Briefly, the cell culture medium was collected and centrifuged at 300× g at 4 °C for 10 minutes, followed by additional centrifugation steps at 2,000× g and 10,000× g at 4 °C for 20 and 30 minutes, respectively. Following resuspension with PBS, the pelleted C-lEVs were washed by recentrifugation at 10,000× g for 30 minutes at 4 °C.

Transmission electron microscopy (TEM) analyses were performed by the 120 kV transmission electron microscope (Hitachi HT-7800, Tokyo, Japan). In brief, 10 µL C-lEVs were loaded on a copper grid placed on ice for 1 minute. 10 µL of phosphotungstic acid was applied to the copper grid for 1 minute for negative staining. The grid was air-dried for several minutes before TEM imaging at 120 kV.

The size and concentration of C-lEVs were analyzed using nanoparticle tracking analysis (NS300, Malvern, UK). Following the manufacturer's instructions, the NTA instrument was set up. The C-lEV samples were diluted to 1 mL with PBS and analyzed at room temperature.

## 2.3 RT-qPCR

RNA was isolated from cells or heart tissue by adding Trizol Reagent (AG21101, Accurate Biology), then separated by adding chloroform and centrifugation. With a reverse transcription kit Evo M-MLV RT (AG11707, Accurate Biology), 1 µg total RNA was converted into cDNA. RT-qPCR reactions were performed on a ROCHE 480II using the SYBR® Green qPCR Kit (AG11701, Accurate Biology) and appropriate primers. Primer sequences are provided in Supplementary Table S1.

## 2.4 Western blot analysis

The cell and C-lEV proteins were obtained by adding RIPA lysis buffer supplemented with protease and phosphatase inhibitors (Beyotime Biotechnology, CN). Proteins were quantified by a BCA assay kit. After adding loading buffer, the sample was heated to 95 °C for 10 minutes to induce denaturation. Identical protein amounts were resolved using SDS-PAGE and then transferred to PVDF membranes (Millipore, USA). The membrane was blocked with 5% non-fat milk for 1–2 hours at room temperature, followed by overnight incubation at 4 °C with specific antibodies on a skaker. Membranes were then incubated with HRP-conjugated secondary antibodies, and immunoblots were visualized using Pierce ECL reagent (Thermo Fisher) through chemiluminescence. Antibodies used included Calnexin (A15631, ABclonal, 1:1000), TSG101 (ab125011, Abcam, 1:2000), β-actin (#sc47778, Santa Cruz Biotechnology, 1:3000), CD63 (ab217345, Abcam, 1:1000), Tubulin (ab6160, Abcam, 1:5000), p-p38 (4511T, Cell Signaling Technology, 1:1000), p38 (ab170099, Abcam, 1:2000), GAPDH (10494-1-AP, Proteintech, 1:5000), and PP2A (81G5, Cell Signaling Technology, 1:1000).

## 2.5 *In vitro* cellular uptake of C-lEVs

Following the manufacturer's instructions, C-lEVs labeled with DiI fluorochrome (C1991S, Byotime) were prepared. RAW264.7 cells were stained with Actin-Tracker Green-488 (C2201S, Byotime) for 10 minutes at 37 °C and incubated with fluorescently labeled C-lEVs for 30 minutes. Cells were fixed with 4% paraformaldehyde and stained with DAPI (Sigma-Aldrich, #D9542). Using an EVOS M7000 fluorescence microscope (Invitrogen, Massachusetts, USA), images were observed.

## 2.6 Flow cytometry

RAW264.7 cells were collected and counted using an automated cell counter (CountessTM3, Thermo Fisher). $10^6$ cells were blocked with 1% bovine serum albumin (BSA, Gibco) to prevent non-specific binding, followed by incubating at 4 °C for 30 minutes with PE-CD86 monoclonal antibody (1:100; 561963, BD Biosciences). To stain with the CD206 antibody, cells were fixed and permeabilized with the intracellular staining kit (00-5523-00, eBioscience) after blocking Fc receptors, as the epitope is located in the medial segment of the cell membrane. Subsequently, PE-CD206

(1:400; 2535977, eBioscience[TM]) staining was performed. Following staining, the cells were rinsed twice with 1% BSA and examined using a flow cytometer (ATTUNE NXT, Thermo Fisher).

## 2.7 Cell proliferation assay

Cell proliferation was assessed with a CCK-8 kit. Briefly, $2 \times 10^4$ cells/well per 100 μL was seeded into 96-well plates. 24 hours after the plates were planted, each group of cells was subjected to fluid exchange with the treatment of PBS, LPS, and LPS+C-lEVs, respectively. Following a 10-hour treatment, each well received 10 μL of CCK8 reagent (Dojindo, Kumamoto, Japan) and was further incubated for 2 hours. Absorbance measurements at 450 nm were performed on a TECAN Spark microplate reader.

## 2.8 Detection of reactive oxygen species

The intracellular ROS level was measured with dichlorofluorescein diacetate (DCFH-DA) green dye. RAW264.7 cells subjected to various treatments were incubated at 37 °C for 45 min with 20 μM DCFH-DA (Beyotime Biotechnology, China; #S0033S) for staining, followed by PBS washing. Then the fluorescent intensity of cells was detected with a flow cytometer (AttuneNxT, Thermo Fisher Scientific, Massachusetts, USA) and analyzed using FlowJo 10.8.1 software.

## 2.9 Animal experiment

The Coxsackievirus B3 (CVB3, Nancy strain, USA) was amplified in Hep2 cells with titter measured via the 50% tissue culture infection dose ($TCID_{50}$) method. The Animal Experimental Ethics Committee of Shandong Provincial Hospital approved the study's animal experimental protocols (NSFC: 2024-178). SPF grade BALB/c male mice (18–20 g, 4 weeks old) were purchased from Beijing Vital River Laboratory Animal Technology Co., Ltd. and kept in a specific pathogen-free conditions. After a 3-day adaptive feeding period, mice were randomly assigned to one of three groups: the normal control group (NC), the CVB3 group, or the CVB3+C-$lEV_{LPS}$ group. A dose of 200 μL $10^4$ $TCID_{50}$ CVB3 was given to mice by intraperitoneal injection to set up viral myocarditis model, whereas the NC group received 200 μL PBS administration intraperitoneally. To investigate the effect of C-$lEV_{LPS}$, a dose of 150 μL C-$lEV_{LPS}$ ($1 \times 10^8$ particles/mL) was administered via the tail vein day 1 and day 3 following the establishment of the viral myocarditis model. Seven days after virus or PBS injection, echocardiography was performed on the mice in each group using M-mode ultrasound (SiliconWave 60, Kolo Medical Co., Ltd., Suzhou, China) to measure the ejection fraction (EF) and fractional shortening (FS) of the left ventricle. Then all mice were anesthetized, blood samples were collected in EDTA tubes, and myocardial tissue was fixed with 4% paraformaldehyde.

## 2.10 Enzyme-linked immunosorbent assay

ELISA analysis was conducted to evaluate the level of cardiac biomarker cardiac troponin (cTnT) in mice plasma. Plasma samples were centrifuged at 1,000× g at 4 °C for 15 minutes within 30 minutes of collection, and the supernatant was collected. cTnT detection was performed using a mouse ELISA kit (ReedBiotech, RE1358M) following the manufacturer's instructions.

## 2.11 Hematoxylin-eosin and immunohistochemistry staining

Heart samples fixed with 4% paraformaldehyde were embedded in paraffin and sectioned into 5 μm white pieces. After staining with hematoxylin-eosin, samples were observed under an optical microscope. Immunohistochemistry staining was performed as previously described (35), the paraffin-embedded heart tissue was cut into 5 μm thick sections, dewaxed and rehydrated, and after antigen repair, the endogenous catalase was blocked. The slide was sealed with 1% BSA for 30 minutes, incubated with CD86 primary antibody overnight, washed, treated with a biotin-coupled secondary antibody for 30 minutes, and observed under a microscope following DAB staining. The CD206 antibody, targeting an epitope in the medial cell membrane segment, was incubated with 0.2% Triton X-100 following BSA blocking to permeabilize the membrane for antibody staining for 15 minutes. Myocardial lesion severity was scored as follows: 0 = no inflammation; 1 = 1–5 inflammatory foci (≤5% area); 2 = >5 foci or >5-20% area involvement; 3 = diffuse inflammation (>20% area), no necrosis; 4 = diffuse inflammation with necrosis.

## 2.12 PolyA-Selected mRNA-Seq

RNA was isolated by adding chloroform followed by centrifugation. Quality assessment involved agarose gel electrophoresis, Nanodrop spectrophotometry, and Qubit fluorometry. Library preparation was streamlined using a kit that combined double-strand synthesis, end repair, and dA-tailing. mRNA was enriched with VAHTS mRNA Capture Beads, fragmented, and then reverse transcribed into cDNA (9, 36). The cDNA was purified, and sequencing adapters were ligated. Library quality was assessed using the Agilent Bioanalyzer and Qubit fluorometer. Sequencing was conducted on an Illumina Novaseq6000 platform in paired-end 150 mode. This protocol generated high-quality sequencing data suited for subsequent bioinformatic analysis.

Raw data was processed with fastp (version 2.0), which removed adapter sequences, trimmed low-quality bases (quality score < 20), and filtered out reads containing more than 10% ambiguous nucleotides (N). The resulting data was referred to as clean data. These clean reads were mapped to the reference genome with HISAT2 (version 2.1.0), and the alignment quality was evaluated

with RSeQC (version 3.0.1). Gene expression levels were quantified with StringTie, and differentially expressed genes were identified through DESeq2 analysis (9).

## 2.13 NanoLC-MS/MS analysis

Peptides (200 ng) were analyzed using a nano-UPLC (nanoElute2) coupled with a timsTOF Pro2 mass spectrometer (Bruker) equipped with a nano-electrospray ion source. A PePSep C18 reversed-phase column (1.9 µm, 75 µm × 15 cm, Bruker, Germany) was used for the separation. The mobile phases were $H_2O$ with 0.1% FA (phase A) and ACN with 0.1% FA (phase B). The sample was separated using a 60-minute gradient at a flow rate of 300 nL/min. Gradient B: 2% for 0 minutes, increasing to 22% over 45 minutes, then to 37% over 5 minutes, further to 80% over another 5 minutes, and maintained at 80% for 5 minutes (37).

Data acquisition is performed in DDA PaSEF mode, with an MS1 scanning range between 100 and 1700 m/z. In PASEF MS/MS scanning, the impact energy rises linearly with ion mobility, starting at 20 eV for $1/K0 = 0.6$ Vs/cm$^2$ and reaching 59 eV for $1/K0 = 1.6$ Vs/cm$^2$.

## 2.14 Protein identification and quantification

The vendor's raw MS files were analyzed with SpectroMine software (v4.2.230428.52329) with the integrated Pulsar search engine. MS spectra were searched against a species-specific UniProt FASTA database (Rattus.fasta) with fixed carbamidomethylation and variable oxidation and N-terminal acetylation. Trypsin was utilized as a protease. A maximum of 2 missed cleavages was permitted. Both PSM and peptide levels were set at 0.01 false discovery rate. Peptide identification was conducted with an initial precursor and fragment mass deviation of up to 20 ppm. All other parameters were kept as default.

## 2.15 Statistical analysis

The data were statistically analyzed and plotted by GraphPad Prism9 software. $p$-values were calculated using Student's $t$-test or one-way ANOVA. $p < 0.05$ was deemed statistically significant. All experiments were conducted a minimum of three times.

# 3 Results

## 3.1 Characterization of C-lEVs

The rat cardiomyocyte cell line H9C2 was used for the isolation of C-lEVs. Following LPS treatment, there was a significant increase in inflammatory cytokines such as IL-6, IL-1β, and TNF-α, accompanied by a decrease in cell viability (Supplementary Figure S1).

Differential centrifugation was used to isolate C-lEV$_{PBS}$ and C-lEV$_{LPS}$ from the culture medium (Figure 1A). Western blot analysis confirmed the presence of C-lEV markers TSG101, CD63, and Actin, while Calnexin was absent (Figure 1B). TEM revealed the typical membranous cup-shaped morphology of both C-lEV$_{PBS}$ and C-lEV$_{LPS}$ (Figures 1C, D). NTA-determined particle sizes predominantly ranged from 100 to 500 nm, with peak sizes of 158 nm for C-lEV$_{PBS}$ and 171.6 nm for C-lEV$_{LPS}$ (Figures 1E, F). Additionally, the particle numbers of C-lEV$_{LPS}$ per milliliter of culture medium were significantly elevated compared to C-lEV$_{PBS}$ (Figure 1G).

## 3.2 *In vitro* studies demonstrate the anti-inflammatory properties of C-lEV$_{LPS}$

The *in vitro* effects of C-lEV$_{LPS}$ were examined with the murine macrophage cell line RAW264.7. The internalization of C-lEV$_{LPS}$ by RAW264.7 cells was evaluated first. Dil fluorescent dye-labeled C-lEV$_{LPS}$ were incubated with RAW264.7 cells for 6 hours. As depicted in Figure 2A, C-lEV$_{LPS}$ could be taken up by RAW264.7 cells. Emerging evidence indicated that activated macrophages can release ROS and pro-inflammatory cytokines such as TNF-α, IL-1β, and IL-6 (38). Herein, RAW264.7 cells were treated with LPS and subsequently exposed to varying concentrations of C-lEV$_{PBS}$ or C-lEV$_{LPS}$. Flow cytometry results indicated that ROS levels were significantly elevated upon treatment with LPS, while C-lEV$_{LPS}$ reversed the LPS-induced increase in ROS ($p$=0.000034, Figure 2B). The expression levels of inflammatory cytokines TNF-α, IL-6, and IL-1β were significantly elevated in LPS-induced RAW264.7 cells (Figures 2C-E). Different C-lEV$_{LPS}$ concentrations resulted in varying decreases in inflammatory cytokine expression. Notably, the $10^7$ particles/mL C-lEV$_{LPS}$ group exerted the most potent effect, significantly suppressing the expression of all inflammatory cytokines tested (Figures 2C-E). Additionally, increased cell proliferation was observed following LPS stimulation, which was suppressed by C-lEV$_{LPS}$ treatment (Supplementary Figure S2). In contrast, different concentrations of C-lEV$_{PBS}$ did not influence the expression of inflammatory cytokines (Supplementary Figure S3). Taken together, C-lEV$_{LPS}$ decreased the expression of inflammatory cytokines compared to C-lEV$_{PBS}$ (Figures 2F-H). These data indicate that C-lEV$_{LPS}$ treatment exerts anti-inflammatory effects on macrophages.

## 3.3 C-lEV$_{LPS}$ alleviated CVB3-induced myocarditis in mice

To evaluate the role of C-lEV$_{LPS}$ in myocarditis, BALB/c mice were injected with CVB3 to induce viral myocarditis. On days 1 and 4 post-CVB3 injection, the mice were administered 150 µL of C-lEV$_{LPS}$ ($10^8$ particles/mL) or PBS (carrier solution) via tail vein injection (Figure 3A). As expected, C-lEV$_{LPS}$ accumulated in the mouse hearts after tail vein injection (Supplementary Figure S4). On day 7, C-lEV$_{LPS}$ mildly reversed the weight loss observed after
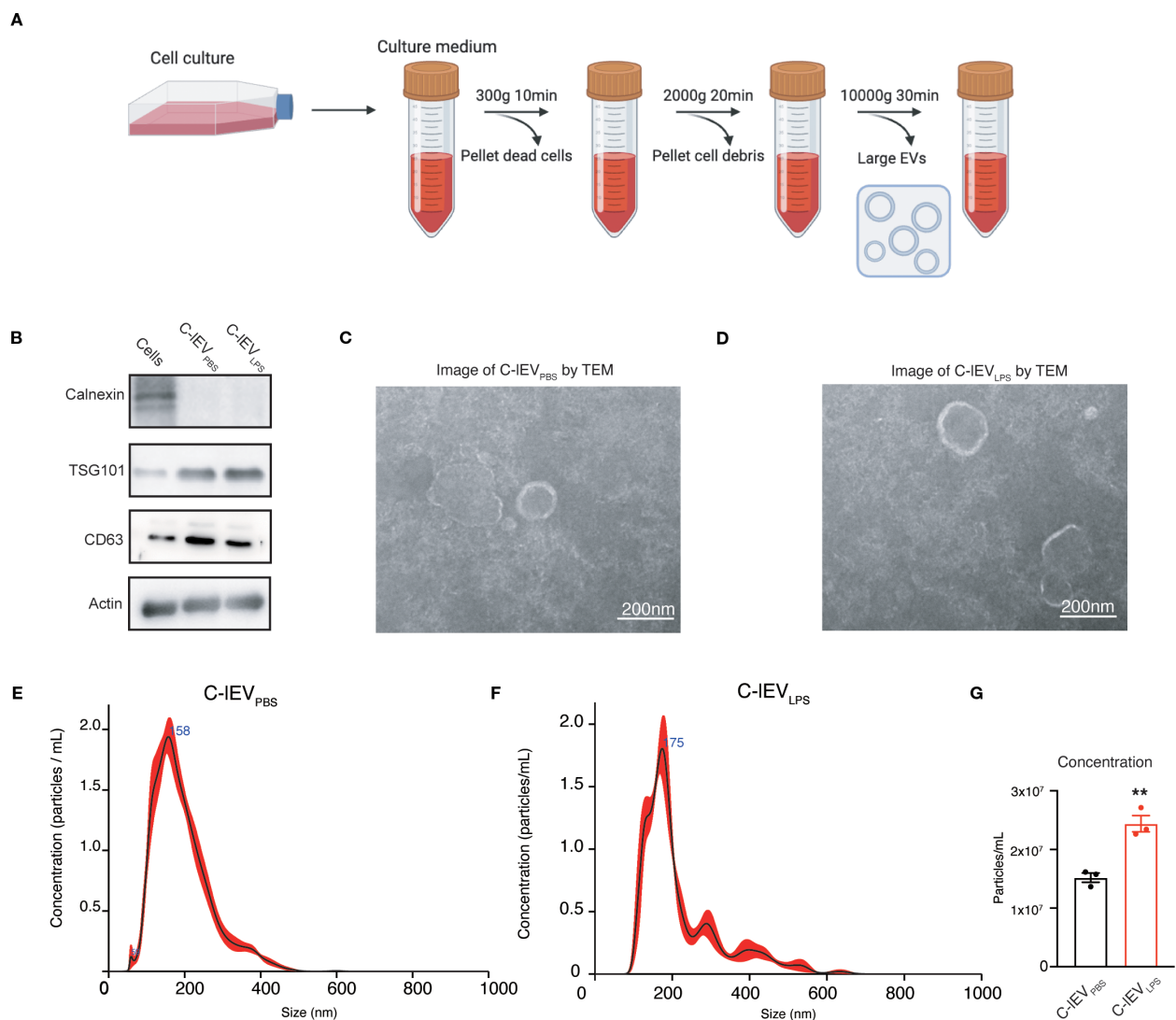
FIGURE 1
Isolation and characterization of C-lEVs. **(A)** Workflow schematic for the isolation of C-lEVs. **(B)** Western blot analysis of Calnexin and C-lEVs markers of TSG101, CD63, and Actin. **(C, D)** Representative images of C-lEV$_{PBS}$ and C-lEV$_{LPS}$ by TEM, scale bars: 200 nm. **(E, F)** Size distribution of C-lEV$_{PBS}$ and C-lEV$_{LPS}$. **(G)** Particle concentration of C-lEV$_{PBS}$ and C-lEV$_{LPS}$. **$p < 0.01$ vs. C-lEV$_{PBS}$ group.

CVB3 infection (Figure 3B). Thus, cardiac function was assessed by echocardiography. As expected, mice induced by CVB3 exhibited cardiac dysfunction, as evidenced by decreased ejection fraction (EF) ($p=0.0003$) and fractional shortening (FS) ($p=0.0005$). Strikingly, the cardiac dysfunction was remarkably attenuated upon treatment with C-lEV$_{LPS}$ (Figure 3C). However, there were no significant differences in left ventricular posterior wall thickness (LVPW) or left ventricular mass (LV mass Cor) between the CVB3 group and the C-lEV$_{LPS}$ group (Supplementary Figure S5). In addition, Kaplan–Meier survival analysis showed no statistically significant differences in survival rates among these groups during the observation period (Supplementary Figure S5).

Then the myocardial tissue was collected. The myocardial surfaces of mice in the NC group appeared smooth, while mice with viral myocarditis showed patch-like lesions in the heart.

Notably, upon treatment with C-lEV$_{LPS}$, the area of patch-like lesions was significantly reduced in the heart (Figure 3D). H&E staining indicated significantly higher pathology scores in the CVB3 group of mice compared to the NC group, while the CVB3 + C-lEV$_{LPS}$ group exhibited notably reduced scores relative to the CVB3 group (Figure 3E). IHC staining and RT-qPCR analysis showed that TNF-α, IL-6, and IL-1β expressions were significantly elevated in the hearts of the mice in the CVB3 group compared to the NC group. Conversely, these cytokine expressions were reduced significantly in the CVB3 + C-lEV$_{LPS}$ group compared to the CVB3 group (Figures 3F-K). Additionally, ELISA analysis revealed that plasma cTnT levels were significantly elevated in CVB3-infected mice and markedly decreased in the CVB3 with C-lEV$_{LPS}$ group (Figure 3L). Collectively, these results indicate that C-lEV$_{LPS}$ treatment reduces the inflammatory response in myocarditis.
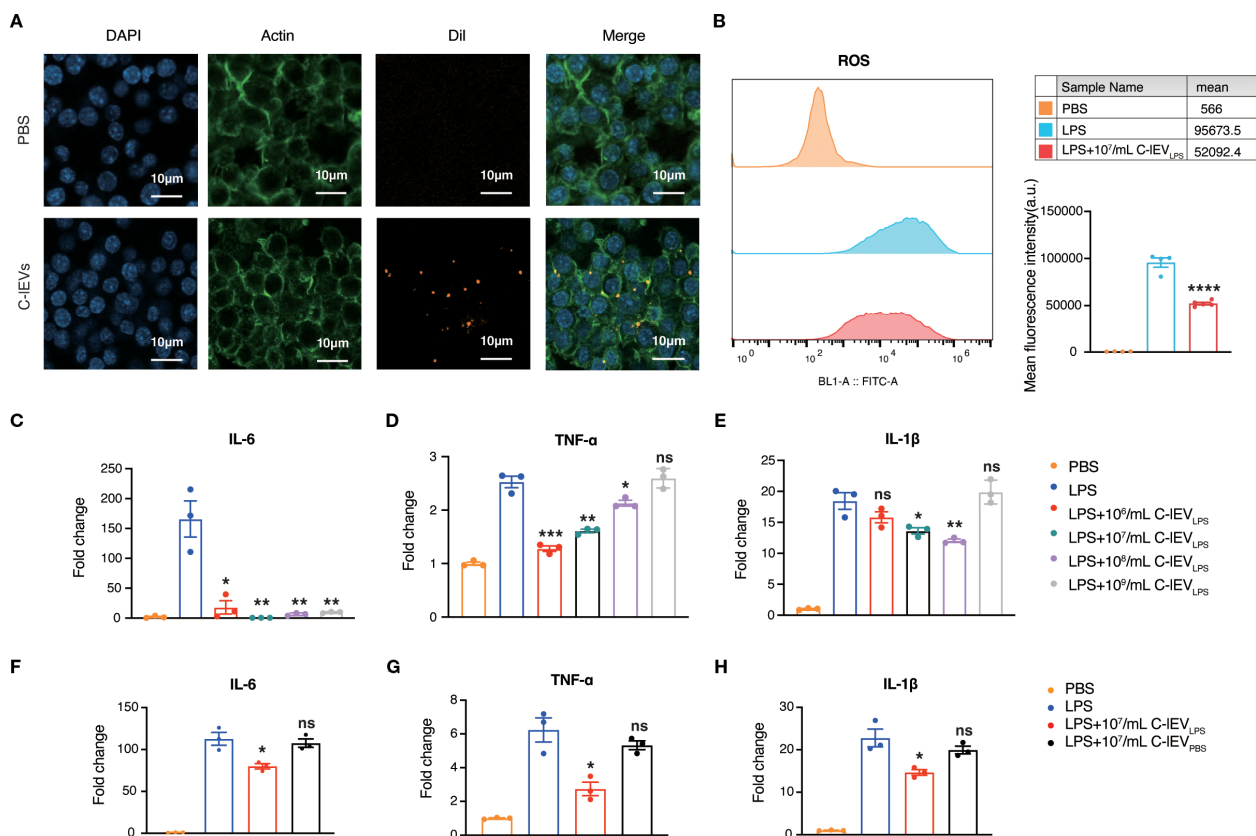
**FIGURE 2**

C-lEV$_{LPS}$ suppressed LPS–stimulated inflammation in RAW 264.7 cells. **(A)** Representative images of RAW 264.7 cells internalizing C-lEV$_{LPS}$, scale bar: 10 µm. **(B)** ROS production in RAW264.7 cells. **(C-H)** The expression levels of IL-6, TNF-α, and IL-1β in RAW264.7 cells determined by RT-qPCR under different treatments. *$p < 0.05$, **$p < 0.01$, ***$p < 0.001$, ****$p < 0.0001$, ns, nonsignificant difference vs. PBS group.

## 3.4 C-lEV$_{LPS}$ induces macrophage polarization from M1 toward M2

Macrophages are crucial in the early development of myocarditis as the main inflammatory and infiltrating cells (5, 7). They can differentiate into pro-inflammatory M1 or anti-inflammatory M2 phenotypes based on the cardiac environment (39). Flow cytometry was used to evaluate macrophage phenotypes and determine if C-lEV$_{LPS}$ reduces inflammation by influencing macrophage polarization. The results indicated that the proportion of CD86-positive M1 macrophages significantly increased after LPS treatment, whereas C-lEV$_{LPS}$ treatment reduced this proportion ($p$=0.008, Figures 4A, B). Conversely, the proportion of CD206-positive M2 macrophages increased after LPS treatment and was further elevated with C-lEV$_{LPS}$ treatment ($p$=0.0049, Figures 4C, D).

Additionally, to verify whether C-lEV$_{LPS}$ could influence macrophage polarization *in vivo*, we performed IHC staining of CD86 and CD206 on the myocardial tissues in the mice. C-lEV$_{LPS}$ treatment modulated macrophage infiltration, reducing the presence of M1 macrophages while enhancing the recruitment of M2 macrophages (Figures 4E-H). These findings suggest that C-lEV$_{LPS}$ treatment induced macrophage polarization toward an M2-like phenotype while inhibiting M1 polarization.

## 3.5 C-lEV$_{LPS}$ regulates macrophage polarization via the p38 MAPK pathway

To elucidate the mechanism by which C-lEV$_{LPS}$ regulates macrophage polarization, RNA sequencing was conducted to identify gene expression differences in macrophages upon treatment with or without C-lEV$_{LPS}$. The volcano plot analysis revealed 941 upregulated genes ($p < 0.05$, log$_2$FC > 0.5) and 1048 downregulated genes ($p < 0.05$, log$_2$FC < −0.5) (Figure 5A).

Notably, gene ontology (GO) analysis of differentially expressed genes indicated significant enrichment of the MAPK pathway (Figure 5B). Given that the p38 MAPK pathway is involved in macrophage polarization (40, 41), we hypothesized that C-lEV$_{LPS}$ modulates macrophage polarization through the p38 MAPK pathway. Blot analysis demonstrated that LPS increased p38 phosphorylation, an effect reversed by C-lEV$_{LPS}$, pointing to C-lEV$_{LPS}$-mediated inhibition of the p38 MAPK pathway (Figures 5C, D).

To confirm that C-lEV$_{LPS}$ influences macrophage polarization through the p38 MAPK pathway, LPS-preconditioned RAW264.7 cells were co-cultured with C-lEV$_{LPS}$ and the p38 MAPK agonist AM. RT-qPCR analysis demonstrated that treatment with C-lEV$_{LPS}$ significantly reduced the levels of pro-
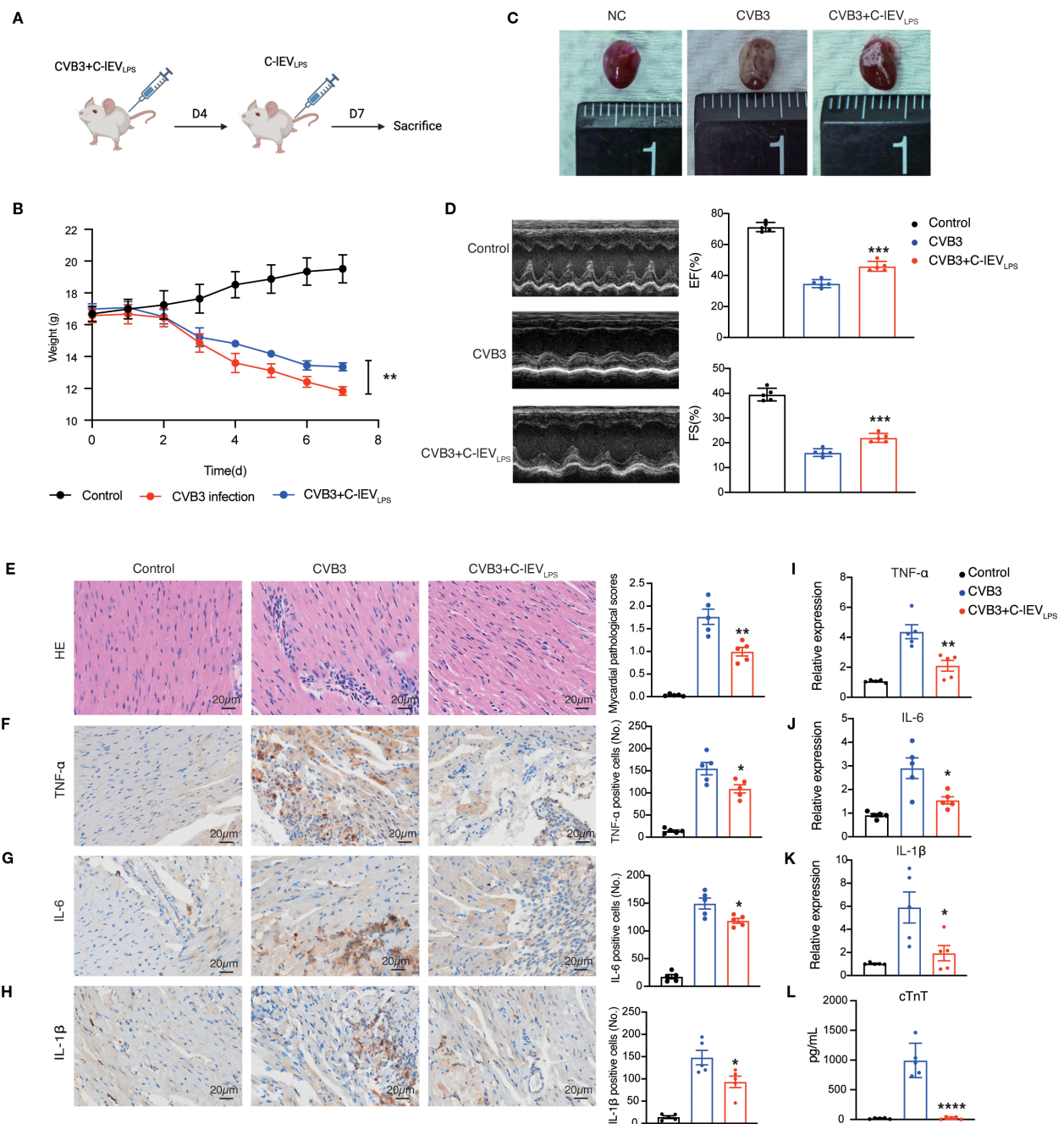
**FIGURE 3**

C-lEV_LPS treatment relieved CVB3-induced myocarditis *in vivo*. **(A)** Animal treatment illustration. **(B)** Appearance of the heart after different treatments. **(C)** Changes in mice body weight among different treatment groups. **(D)** Left panel, representative echocardiographic images of the mice. Right panel, statistical analysis results of left ventricular EF and FS. **(E)** HE staining images and pathological scores of myocardial tissues, scale bar: 20 μm. **(F-H)** Analysis of immunohistochemical staining for inflammatory cytokines expression and semiquantitative histological analysis, scale bar: 20 μm. **(I-K)** The expression levels of TNF-α, IL-6, and IL-1β in mice myocardial tissue. **(L)** The serum levels of cTnT in mice. (n = 5) *$p < 0.05$, **$p < 0.01$, ***$p < 0.001$, ****$p < 0.0001$ vs. CVB3 group.

inflammatory cytokines IL-6, IL-1β, and TNF-α compared to the LPS group. However, co-treatment with AM eliminates the anti-inflammatory effects of C-lEV_LPS (Figures 5E–G). Flow cytometry analysis showed that treatment with C-lEV_LPS significantly increased the proportion of CD206-positive M2 macrophages and decreased the proportion of CD86-positive M1 macrophages compared to the LPS group. Notably, the addition of AM reversed the effects of C-lEV_LPS, which reduced the proportion of M2 macrophages and increased M1 macrophages (Figures 5H–K). Collectively, these findings suggest that C-lEV_LPS modulates macrophage polarization, at least in part, through the p38 MAPK signaling pathway.
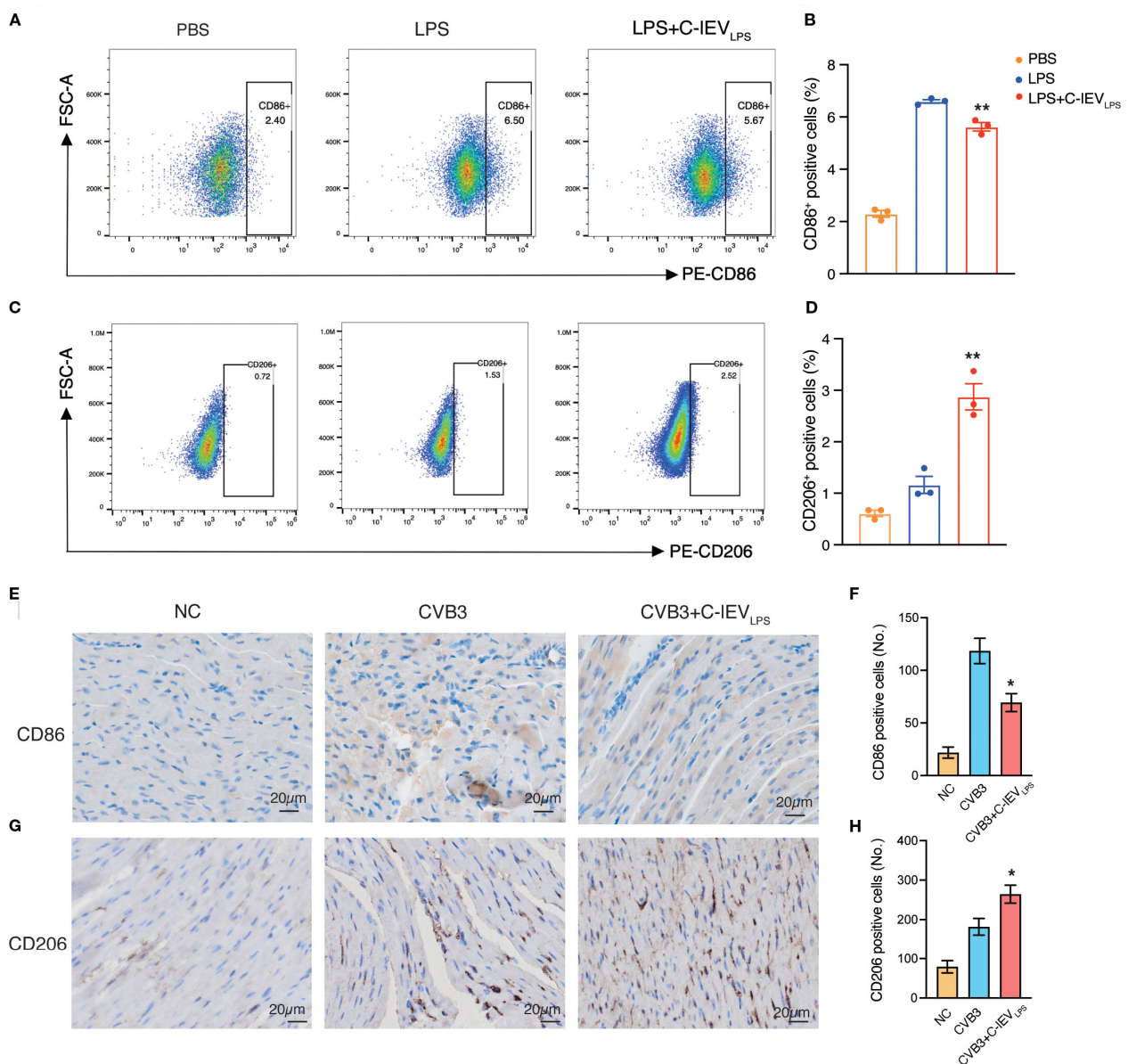
**FIGURE 4**

C-lEV$_{LPS}$ treatment regulated macrophage polarization both *in vitro* and *in vivo*. **(A, B)** Flow cytometry analysis of CD86 positive RAW 264.7 cells and quantitative data analysis. **(C, D)** Flow cytometry analysis of CD206 positive RAW 264.7 cells and quantitative data analysis. **(E, F)** Analysis of immunohistochemical staining for CD86 and semiquantitative histological analysis (n=5), scale bar: 20 μm. **(G, H)** Analysis of immunohistochemical staining for CD206 and semiquantitative histological analysis (n=5), scale bar: 20 μm. *$p < 0.05$, **$p < 0.01$ vs. LPS or CVB3 group.

## 3.6 PP2AA serves a potential regulator from C-lEV$_{LPS}$ mediating macrophage polarization

EVs are known to contain multiple proteins relevant to various biological processes (34). Based on label-free proteomics analysis, C-lEV$_{LPS}$ and C-lEV$_{PBS}$ exhibited distinct protein compositions, with 824 and 580 proteins identified, respectively (Figure 6A). Then GO analyses of biological processes and reactome gene set analysis were performed. GO biological process analysis (Figure 6B) revealed that the "peptide metabolic process" was enriched in C-

lEV$_{LPS}$ proteins significantly. Reactome gene set analysis revealed that these proteins are associated with several signaling pathways, particularly those involved in regulating the inflammatory response, including the "RAF/MAPK kinase cascade", "Adaptive immune system", "TCR signaling", "MAPK6/MAPK4 signaling", and "NIK-noncanonical NF-κB signaling" pathways (Figure 6C).

Among the proteins associated with the "RAF/MAPK kinase cascade", Ppp2r1a was identified as upregulated in C-lEV$_{LPS}$ (Figure 6D), which was validated by Western blot analysis (Figure 6E). Ppp2r1a encodes PP2AA, a subunit of protein phosphatase 2A (PP2A), an important serine-threonine
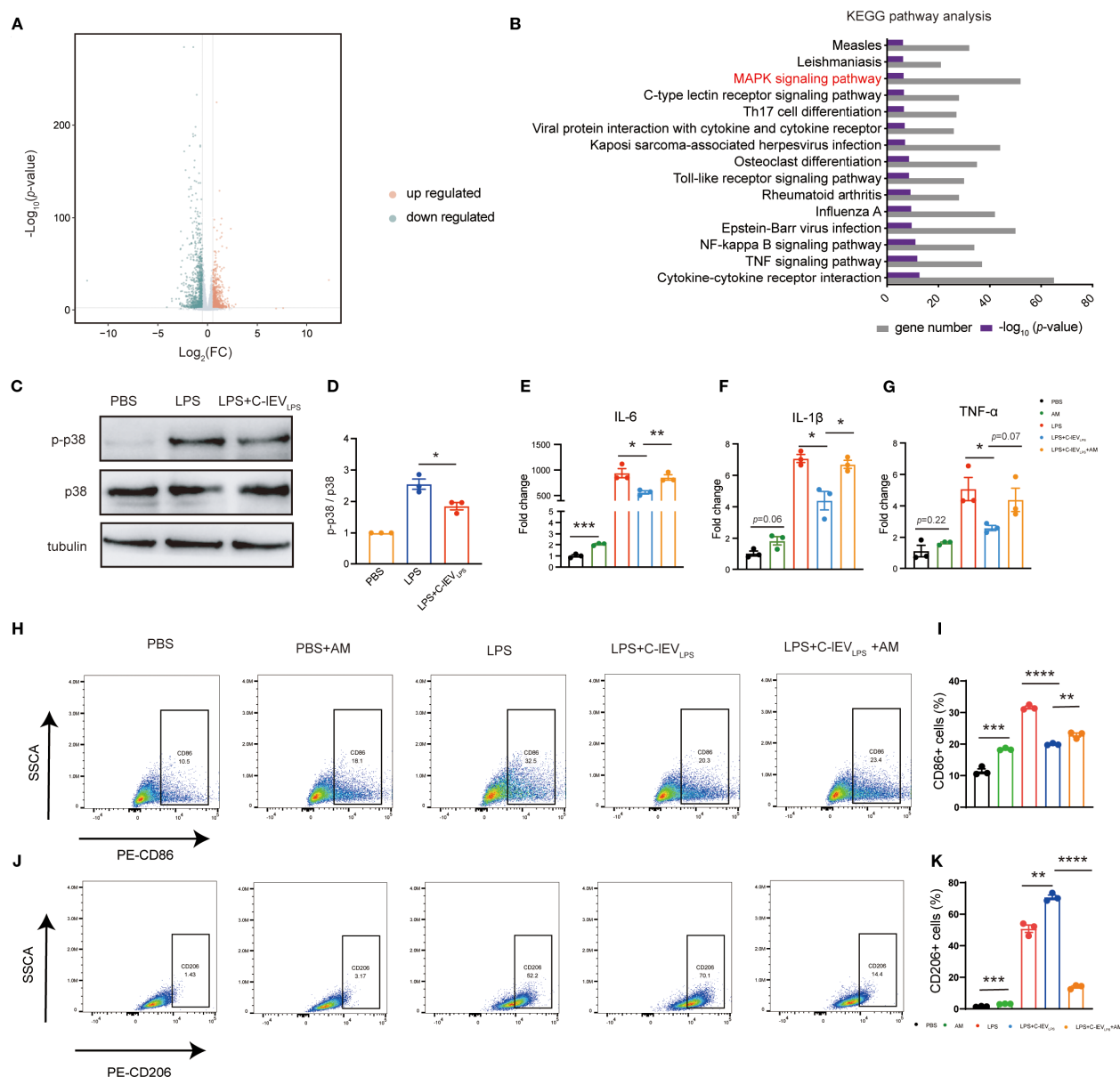
**FIGURE 5**

C-lEV$_{LPS}$ regulates macrophage polarization by the p38 MAPK pathway. **(A, B)** Transcriptomic alterations in LPS-stimulated RAW 264.7 cells following treatment with C-lEV$_{LPS}$ revealed by RNA-seq analysis. **(C, D)** Representative bands of p-p38/p38 levels by Western blot, with semiquantitative analysis, in RAW 264.7 cells subjected to various treatments. **(E-G)** Expression levels of pro-inflammatory gene profiles in RAW 264.7 cells. **(H, I)** Flow cytometry analysis of CD86-positive RAW 264.7 cells and quantitative data analysis. **(J, K)** Flow cytometry analysis of CD206-positive RAW 264.7 cells and quantitative data analysis. $*p < 0.05$, $**p < 0.01$, $***p < 0.001$, $****p < 0.0001$.

phosphatase capable of dephosphorylating p38 MAPK. It has been reported that PP2AA can recruit other subunits of PP2A (42). Therefore, we hypothesized that the upregulated PP2AA in C-lEV$_{LPS}$ is delivered to macrophages, where it recruits additional PP2A subunits to dephosphorylate p38 MAPK.

To confirm that C-lEV$_{LPS}$ transports PP2AA to macrophages, RAW264.7 cells were incubated with C-lEV$_{LPS}$ for 12 hours. Western blot showed a significant increase in PP2AA expression in RAW264.7 cells treated by C-lEV$_{LPS}$ (Figure 6F). Overall, these data indicate that C-lEV$_{LPS}$ has the capability to deliver PP2AA to

macrophages, thereby promoting the formation of PP2A complexes, which may subsequently dephosphorylate p38 MAPK.

To further confirm that the effects of C-lEV$_{LPS}$ are mediated through PP2A, LPS-preconditioned RAW264.7 cells were co-cultured with C-lEV$_{LPS}$ and the PP2A inhibitor LB-100. Western blot analysis revealed that C-lEV$_{LPS}$ reduced the phosphorylation level of p38 after LPS stimulation, while the use of LB-100 diminished this effect (Figure 6G). Meanwhile, RT-qPCR analysis revealed that treatment with C-lEV$_{LPS}$ significantly reduced the mRNA expression of pro-inflammatory cytokines IL-6, IL-1β, and
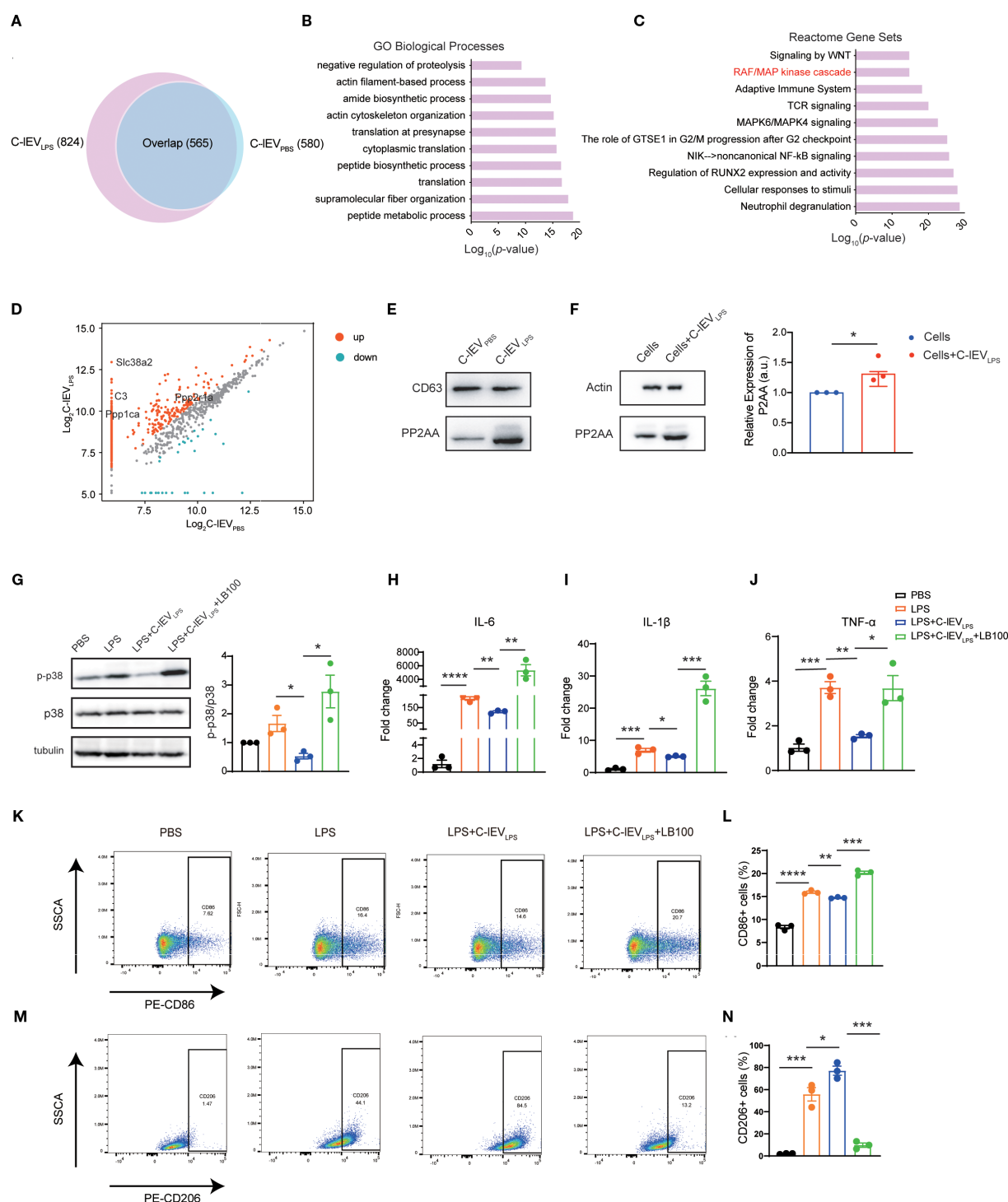
**FIGURE 6**

C-lEV$_{LPS}$ encapsulates PP2AA and regulates the p38-MAPK pathway of macrophage by synthesizing PP2A. **(A)** Venn diagram depicting the common and total proteins in C-lEV$_{LPS}$ vs. C-lEV$_{PBS}$. **(B)** Gene ontology analysis of proteins enriched in C-lEV$_{LPS}$ focused on biological processes. **(C)** Reactome pathway analysis conducted on proteins enriched in C-lEV$_{LPS}$. **(D)** Volcano plot illustrating the differentially enriched proteins in C-lEV$_{LPS}$ vs C-lEV$_{PBS}$. **(E)** Representative bands of PP2A and CD63 in C-lEV$_{LPS}$ and C-lEV$_{PBS}$ by Western blot. **(F)** Western blot showing PP2A and actin expression in RAW264.7 cells. **(G)** Representative bands of p-p38/p38 levels by Western blot, with semiquantitative analysis, in RAW 264.7 cells subjected to various treatments. **(H-J)** Expression levels of pro-inflammatory gene profiles in RAW 264.7 cells. **(K, L)** Flow cytometry analysis of CD86-positive RAW 264.7 cells and quantitative data analysis. **(M, N)** Flow cytometry analysis of CD206-positive RAW 264.7 cells and quantitative data analysis. $*p < 0.05$, $**p < 0.01$, $***p < 0.001$, $****p < 0.0001$.

TNF-α in LPS-stimulated RAW264.7 cells compared to the LPS group. Importantly, co-treatment with LB-100 eliminates the anti-inflammatory effects of C-lEV$_{LPS}$ (Figures 6H–J).

Flow cytometry results showed that treatment with C-lEV$_{LPS}$ decreased the proportion of CD86-positive M1 macrophages (Figures 6K, L) and increased the proportion of CD206-positive M2 macrophages (Figures 6M, N) relative to the LPS group. However, the addition of LB-100 reversed these effects resulting in increased percentage of M1 macrophages and reduced percentage of M2 macrophages (Figures 6K-N).

Overall, these data indicate that C-lEV$_{LPS}$ has the capability to deliver PP2AA to macrophages, which may subsequently dephosphorylate p38 MAPK and exert anti-inflammatory effects.
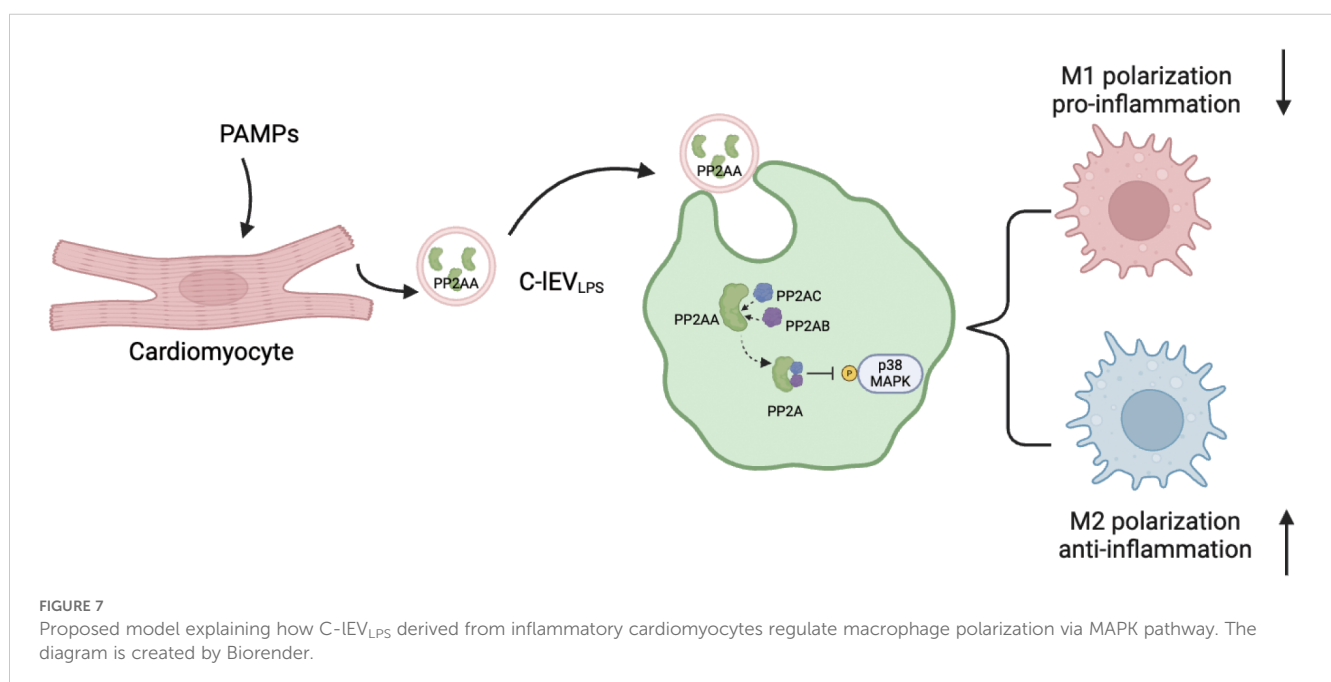
# 4 Discussion

Myocarditis is characterized by the infiltration of various inflammatory cells into myocardial tissue (43, 44), with macrophages being the primary immune cells (5). Viral infections are the main cause of myocarditis (45, 46), where viruses enter cardiomyocytes via virus-specific receptors, activating innate immune responses that include macrophage infiltration (47). However, the fundamental mechanisms underlying the crosstalk between cardiomyocytes and macrophages in myocarditis remain largely unexplored.

Existing literature has shown that EVs can alter the polarization state of macrophages during cardiac injury. For example, sEVs secreted by M2 macrophages promote the conversion of macrophages toward the M2 phenotype in viral myocarditis (48), while sEVs secreted by ischemic cardiomyocytes act on macrophages, modulating their inflammatory cytokine expression profile and enhancing their adhesion to fibronectin (49). However, the effects of lEVs secreted by cardiomyocytes under inflammatory conditions on macrophages remain unexplored. In contrast to previous studies, our research fills this gap by revealing how lEVs derived from inflamed cardiomyocytes influence macrophages in myocarditis.

In this study, the in vitro model employed LPS to stimulate inflammatory signaling, primarily activating the TLR4-NF-κB pathway (50); the in vivo model used CVB3 infection, which triggers cytoplasmic RIG-I-like receptors (51) and, to a lesser extent, TLR4 signaling (52). Although the upstream receptors that initiate the two models differ, the literature has reported that the capsid protein of CVB3 can crosstalk with TLR4 and induce inflammasome activation (52, 53). The choice of LPS for in vitro work was indeed due to CVB3 infection causing extensive cell death and abundant viral release, making it almost impossible to obtain pure, virus-free C-lEVs, whereas LPS-induced sterile inflammation can be readily washed out of C-lEV preparations.

We found that certain doses of C-lEV$_{LPS}$ but not C-lEV$_{PBS}$ inhibited the secretion of inflammatory cytokines in macrophages and ameliorated myocardial inflammation in mice. In addition, our findings indicate that the culture medium of LPS-induced H9C2 cells contained approximately $2–3 \times 10^7$ C-lEVs per milliliter. Similarly, the most effective concentration for macrophages is $10^7$ particles per milliliter, which is comparable to the concentration secreted by cardiomyocytes. Based on our experimental results and current literature, we speculate that only C-lEV$_{LPS}$ at near-physiological concentrations exhibits the expected anti-inflammatory effects, while excessively high doses (e.g., $10^9$/mL) may lose their regulatory capacity. This indicates that the amount of large EVs released by cardiomyocytes under inflammatory conditions is sufficient to alter macrophage polarization. Although these findings provide valuable insights, more detailed mechanistic investigation is needed to thoroughly explain this observation.



FIGURE 7
Proposed model explaining how C-lEV$_{LPS}$ derived from inflammatory cardiomyocytes regulate macrophage polarization via MAPK pathway. The diagram is created by Biorender.

Considering that the normal blood volume of a mouse is approximately 72 mL/kg, a 20 g mouse has a blood volume of approximately 1.44 mL (54). To achieve a concentration of $10^7$ particles/mL in mouse blood, we injected 150 μL of C-lEV$_{LPS}$ at $10^8$ particles/mL, which alleviated myocarditis in mice.

Besides, in this study we found that C-lEV$_{LPS}$ altered the M1/M2 macrophage ratio both *in vivo* and *in vitro*. RNA sequencing suggested that the effects of C-lEV$_{LPS}$ may be mediated through the p38 MAPK pathway, and this was further confirmed by Western blot analysis, which demonstrated that C-lEV$_{LPS}$ could regulate the phosphorylation level of p38. Additionally, proteomic analysis identified an increase in PP2AA, a subunit of PP2A, in C-lEV$_{LPS}$. PP2A is a crucial serine-threonine phosphatase capable of dephosphorylating p38 MAPK. PP2AA exhibits a horseshoe-shaped structure that facilitates the recruitment of other PP2A subunits (42). In addition, the PP2A inhibitor abrogated the anti-inflammatory effects of C-lEV$_{LPS}$. These results suggest that C-lEV$_{LPS}$ regulates the p38 MAPK pathway through PP2A (Figure 7). Taken together, these results suggest that C-lEV$_{LPS}$ regulates the p38 MAPK pathway through PP2A.

Nevertheless, our study has some limitations that should be addressed in future research. First, our study uses LPS to stimulate H9C2 cardiomyocytes *in vitro* and CVB3 to induce myocarditis *in vivo*. Despite possible mechanistic differences, it is technically challenging to obtain C-lEVs completely free of infectious viral particles following CVB3 exposure. Moreover, the recent evidence indicates that CVB3 may also engage TLR4 signaling (52, 53), suggesting an overlap in the downstream pathways activated by CVB3 and LPS. Nonetheless, we recognize that viral myocarditis is more clinically relevant, and our current approach represents a compromise to balance experimental feasibility and mechanistic insight. Future studies employing advanced virus inactivation methods and refined cell models will be necessary to distinguish these mechanisms more clearly.

Second, macrophage polarization is an extremely complex process that is regulated by multiple signaling pathways (49, 55). While our data indicate that the regulatory function of C-lEV$_{LPS}$ is mediated through the MAPK signaling pathway, we acknowledge the potential involvement of additional pathways and do not discount their significance. RNA sequencing revealed that C-lEV$_{LPS}$ modulates numerous pathways, including the NF-κB signaling pathway, which may influence macrophage polarization. Therefore, the immune regulatory mechanisms of C-lEV$_{LPS}$ require further investigation.

Third, we did not assess the long-term effects of C-lEV$_{LPS}$ on myocarditis progression. Myocarditis is a dynamic disease that progresses through three distinct phases: the acute phase (characterized by viral infection and initial inflammatory response), the subacute phase (involving immune-mediated myocardial injury), and the chronic phase (which may lead to fibrosis and dilated cardiomyopathy). Our study focused solely on the acute phase, leaving open the question of whether C-lEV$_{LPS}$ administration could influence later stages, particularly fibrosis and cardiac remodeling. Future studies should evaluate the impact of C-lEV$_{LPS}$ at different disease stages to determine its full therapeutic potential.

Currently, there is no specific therapy for myocarditis, and symptomatic management remains the primary method. Research indicates that lncRNA AK083884 from M2 macrophage exosomes safeguards mice against CVB3-induced viral myocarditis (48). Besides, a recent study suggests that large EVs contain higher levels of cargo molecules, including proteins and RNAs, and have segregated plasma membrane domains compared to small EVs (34). This enhances their likelihood of fusing with target cells. In a study about myocardial infarction, cardiomyocyte-derived large EVs, but not small EVs, modulate the release of CCL2, CCL7, and IL-6 from cardiac monocytes (56). Leveraging a controllable in vitro LPS-induced inflammatory model, we found that inflammation-induced C-lEVs can modulate macrophage polarization and attenuate inflammation both in vitro and in vivo. This suggests that specific cargo proteins within C-lEVs (e.g., PP2A-A) could be extracted and employed as novel intercellular signaling vehicles, providing a potential therapeutic avenue for the treatment of myocarditis.

## Data availability statement

The datasets presented in this study can be found in online repositories. The names of the repository/repositories and accession number(s) can be found below: https://www.ncbi.nlm.nih.gov/geo/, GSE279575 http://www.proteomexchange.org/, PXD057460.

## Ethics statement

The animal study was approved by the animal experimental ethics committee of Shandong Provincial Hospital. The study was conducted in accordance with the local legislation and institutional requirements.

## Author contributions

YJ: Methodology, Conceptualization, Writing – original draft, Formal analysis, Investigation, Data curation. YY: Software, Writing – review & editing, Writing – original draft, Investigation, Conceptualization, Visualization, Funding acquisition, Resources, Project administration, Formal analysis. YX: Data curation, Writing – original draft, Formal analysis, Visualization. SZ: Methodology, Writing – original draft, Formal analysis. MM: Writing – review & editing, Conceptualization. BH: Supervision, Writing – review & editing, Software, Funding acquisition, Project administration.

## Funding

## Acknowledgments

We would like to express our heartfelt gratitude to Kai Guo from the Shandong Provincial Hospital for the technical help and to Qiuyao Jiang from Shandong First Medical University for the guidance. We also thank Lingjun Tong from Shandong First Medical University for his valuable advice, as well as Haidan Wang and Yutong Wei for their assistance in the experiments.

## Conflict of interest

The authors declare that the research was conducted in the absence of any commercial or financial relationships that could be construed as a potential conflict of interest.

## Generative AI statement

The author(s) declare that no Generative AI was used in the creation of this manuscript.

Any alternative text (alt text) provided alongside figures in this article has been generated by Frontiers with the support of artificial intelligence and reasonable efforts have been made to ensure accuracy, including review by the authors wherever possible. If you identify any issues, please contact us.

## Publisher's note

All claims expressed in this article are solely those of the authors and do not necessarily represent those of their affiliated organizations, or those of the publisher, the editors and the reviewers. Any product that may be evaluated in this article, or claim that may be made by its manufacturer, is not guaranteed or endorsed by the publisher.

## Supplementary material

The Supplementary Material for this article can be found online at: https://www.frontiersin.org/articles/10.3389/fimmu.2025.1629676/full#supplementary-material

## References

1. Law YM, Lal AK, Chen S, Čiháková D, Cooper LT Jr., Deshpande S, et al. Diagnosis and management of myocarditis in children: A scientific statement from the american heart association. *Circulation*. (2021) 144:e123–e35. doi: 10.1161/CIR.0000000000001001

2. Sagar S, Liu PP, Cooper LT Jr. Myocarditis. *Lancet (London England)*. (2012) 379:738–47. doi: 10.1016/S0140-6736(11)60648-X

3. Nunes MC, Guimarães Júnior MH, Diamantino AC, Gelape CL, Ferrari TC. Cardiac manifestations of parasitic diseases. *Heart (British Cardiac Society)*. (2017) 103:651–8. doi: 10.1136/heartjnl-2016-309870

4. Francone M, Chimenti C, Galea N, Scopelliti F, Verardo R, Galea R, et al. CMR sensitivity varies with clinical presentation and extent of cell necrosis in biopsy-proven acute myocarditis. *JACC Cardiovasc imaging*. (2014) 7:254–63. doi: 10.1016/j.jcmg.2013.10.011

5. Lasrado N, Borcherding N, Arumugam R, Starr TK, Reddy J. Dissecting the cellular landscape and transcriptome network in viral myocarditis by single-cell RNA sequencing. *iScience*. (2022) 25:103865. doi: 10.1016/j.isci.2022.103865

6. Epelman S, Lavine KJ, Beaudin AE, Sojka DK, Carrero JA, Calderon B, et al. Embryonic and adult-derived resident cardiac macrophages are maintained through distinct mechanisms at steady state and during inflammation. *Immunity*. (2014) 40:91–104. doi: 10.1016/j.immuni.2013.11.019

7. Nahrendorf M, Swirski FK. Monocyte and macrophage heterogeneity in the heart. *Circ Res*. (2013) 112:1624–33. doi: 10.1161/CIRCRESAHA.113.300890

8. Mosser DM, Edwards JP. Exploring the full spectrum of macrophage activation. *Nat Rev Immunol*. (2008) 8:958–69. doi: 10.1038/nri2448

9. Ye T, Chen Z, Zhang J, Luo L, Gao R, Gong L, et al. Large extracellular vesicles secreted by human iPSC-derived MSCs ameliorate tendinopathy via regulating macrophage heterogeneity. *Bioactive Materials*. (2023) 21:194–208. doi: 10.1016/j.bioactmat.2022.08.007

10. Taufalele PV, Wang W, Simmons AJ, Southard-Smith AN, Chen B, Greenlee JD, et al. Matrix stiffness enhances cancer-macrophage interactions and M2-like macrophage accumulation in the breast tumor microenvironment. *Acta Biomaterialia*. (2023) 163:365–77. doi: 10.1016/j.actbio.2022.04.031

11. Yang P, Chen Z, Huang W, Zhang J, Zou L, Wang H. Communications between macrophages and cardiomyocytes. *Cell Communication Signaling: CCS*. (2023) 21:206. doi: 10.1186/s12964-023-01202-4

12. Kumar MA, Baba SK, Sadida HQ, Marzooqi SA, Jerobin J, Altemani FH, et al. Extracellular vesicles as tools and targets in therapy for diseases. *Signal Transduct targeted Ther*. (2024) 9:27. doi: 10.1038/s41392-024-01735-1

13. Memon MA, Shahidan WNS. Evaluating the feasibility of exosome technologies in COVID-19 treatment: navigating the intersection of reality and fantasy perspectives. (2024) 9:amj-23-204. doi: 10.21037/amj-23-204

14. Amirzadeh Gougheri K, Ahmadi A, Ahmadabadi MG, Babajani A, Yazdanpanah G, Bahrami S, et al. Exosomal Cargo: Pro-angiogeneic, anti-inflammatory, and regenerative effects in ischemic and non-ischemic heart diseases - A comprehensive review. *Biomed Pharmacother = Biomed Pharmacother*. (2023) 168:115801. doi: 10.1016/j.biopha.2023.115801

15. Jadli AS, Parasor A, Gomes KP, Shandilya R, Patel VB. Exosomes in cardiovascular diseases: pathological potential of nano-messenger. *Front Cardiovasc Med*. (2021) 8:767488. doi: 10.3389/fcvm.2021.767488

16. Yaghoobi A, Rezaee M, Behnoush AH, Khalaji A, Mafi A, Houjaghan AK, et al. Role of long noncoding RNAs in pathological cardiac remodeling after myocardial infarction: An emerging insight into molecular mechanisms and therapeutic potential. *Biomed Pharmacother = Biomed Pharmacother*. (2024) 172:116248. doi: 10.1016/j.biopha.2024.116248

17. Caño-Carrillo S, Castillo-Casas JM, Franco D, Lozano-Velasco E. Unraveling the signaling dynamics of small extracellular vesicles in cardiac diseases. *Cells*. (2024) 13:265. doi: 10.3390/cells13030265

18. Wang Y, Qiu Z, Yuan J, Li C, Zhao R, Liu W, et al. Hypoxia-reoxygenation induces macrophage polarization and causes the release of exosomal miR-29a to mediate cardiomyocyte pyroptosis. *In Vitro Cell Dev Biol Animal*. (2021) 57:30–41. doi: 10.1007/s11626-020-00524-8

19. Dai Y, Wang S, Chang S, Ren D, Shali S, Li C, et al. M2 macrophage-derived exosomes carry microRNA-148a to alleviate myocardial ischemia/reperfusion injury via inhibiting TXNIP and the TLR4/NF-κB/NLRP3 inflammasome signaling pathway. *J Mol Cell Cardiol*. (2020) 142:65–79. doi: 10.1016/j.yjmcc.2020.02.007

20. Yu X, Deng L, Wang D, Li N, Chen X, Cheng X, et al. Mechanism of TNF-α autocrine effects in hypoxic cardiomyocytes: initiated by hypoxia inducible factor 1α, presented by exosomes. *J Mol Cell Cardiol*. (2012) 53:848–57. doi: 10.1016/j.yjmcc.2012.10.002

21. Yuan W, Liang X, Liu Y, Wang H. Mechanism of miR-378a-3p enriched in M2 macrophage-derived extracellular vesicles in cardiomyocyte pyroptosis after MI. *Hypertension Res: Off J Japanese Soc Hypertension*. (2022) 45:650–64. doi: 10.1038/s41440-022-00851-1

22. Gallet R, Dawkins J, Valle J, Simsolo E, de Couto G, Middleton R, et al. Exosomes secreted by cardiosphere-derived cells reduce scarring, attenuate adverse remodelling, and improve function in acute and chronic porcine myocardial infarction. *Eur Heart J*. (2017) 38:201–11. doi: 10.1093/eurheartj/ehw240

23. Kervadec A, Bellamy V, El Harane N, Arakélian L, Vanneaux V, Cacciapuoti I, et al. Cardiovascular progenitor-derived extracellular vesicles recapitulate the beneficial effects of their parent cells in the treatment of chronic heart failure. *J Heart Lung Transplant: Off Publ Int Soc Heart Transplant*. (2016) 35:795–807. doi: 10.1016/j.healun.2016.01.013

24. El Harane N, Kervadec A, Bellamy V, Pidial L, Neametalla HJ, Perier MC, et al. Acellular therapeutic approach for heart failure: *in vitro* production of extracellular vesicles from human cardiovascular progenitors. *Eur Heart J*. (2018) 39:1835–47. doi: 10.1093/eurheartj/ehy012

25. Welsh JA, Goberdhan DCI, O'Driscoll L, Buzas EI, Blenkiron C, Bussolati B, et al. Minimal information for studies of extracellular vesicles (MISEV2023): From basic to advanced approaches. *J Extracell Vesicles*. (2024) 13:e12404. doi: 10.1002/jev2.12404

26. Cheng L, Hill AF. Therapeutically harnessing extracellular vesicles. *Nat Rev Drug Discov*. (2022) 21:379–99. doi: 10.1038/s41573-022-00410-w

27. Durcin M, Fleury A, Taillebois E, Hilairet G, Krupova Z, Henry C, et al. Characterisation of adipocyte-derived extracellular vesicle subtypes identifies distinct protein and lipid signatures for large and small extracellular vesicles. *J Extracell Vesicles*. (2017) 6:1305677. doi: 10.1080/20013078.2017.1305677

28. Lim HJ, Yoon H, Kim H, Kang YW, Kim JE, Kim OY, et al. Extracellular vesicle proteomes shed light on the evolutionary, interactive, and functional divergence of their biogenesis mechanisms. *Front Cell Dev Biol*. (2021) 9:734950. doi: 10.3389/fcell.2021.734950

29. Gavinho B, Sabatke B, Feijoli V, Rossi IV, da Silva JM, Evans-Osses I, et al. Peptidylarginine deiminase inhibition abolishes the production of large extracellular vesicles from giardia intestinalis, affecting host-pathogen interactions by hindering adhesion to host cells. *Front Cell Infect Microbiol*. (2020) 10:417. doi: 10.3389/fcimb.2020.00417

30. Sproviero D, Gagliardi S, Zucca S, Arigoni M, Giannini M, Garofalo M, et al. Different miRNA profiles in plasma derived small and large extracellular vesicles from patients with neurodegenerative diseases. *Int J Mol Sci*. (2021) 22:2737. doi: 10.3390/ijms22052737

31. Scuteri A, Donzelli E. Dual role of extracellular vesicles in neurodegenerative diseases. *World J Stem Cells*. (2024) 16:1002–11. doi: 10.4252/wjsc.v16.i12.1002

32. Krishnamachary B, Cook C, Kumar A, Spikes L, Chalise P, Dhillon NK. Extracellular vesicle-mediated endothelial apoptosis and EV-associated proteins correlate with COVID-19 disease severity. *J Extracell Vesicles*. (2021) 10:e12117. doi: 10.1002/jev2.12117

33. Jimenez L, Yu H, McKenzie AJ, Franklin JL, Patton JG, Liu Q, et al. Quantitative proteomic analysis of small and large extracellular vesicles (EVs) reveals enrichment of adhesion proteins in small EVs. *J Proteome Res*. (2019) 18:947–59. doi: 10.1021/acs.jproteome.8b00647

34. Cocucci E, Meldolesi J. Ectosomes and exosomes: shedding the confusion between extracellular vesicles. *Trends Cell Biol*. (2015) 25:364–72. doi: 10.1016/j.tcb.2015.01.004

35. Liu X, Li M, Chen Z, Yu Y, Shi H, Yu Y, et al. Mitochondrial calpain-1 activates NLRP3 inflammasome by cleaving ATP5A1 and inducing mitochondrial ROS in CVB3-induced myocarditis. *Basic Res Cardiol*. (2022) 117:40. doi: 10.1007/s00395-022-00948-1

36. Liu Z, Weng T, Cheng M, Lei T, Xiao D, Deng Q, et al. KRT14 knockdown reduces cisplatin resistance by lowering LRP11 expression levels in cisplatin-resistant ovarian cancer cell lines. *Trans Cancer Res*. (2025) 14:1786–98. doi: 10.21037/tcr-24-1795

37. Zhang Y, Zhang Y, Yin R, Fang X, Miao R, Guan H, et al. Multi-omics characterization of type 2 diabetes mellitus-induced gastroenteropathy in the db/db mouse model. *Front Cell Dev Biol*. (2024) 12:1417255. doi: 10.3389/fcell.2024.1417255

38. Sha W, Zhao B, Wei H, Yang Y, Yin H, Gao J, et al. Astragalus polysaccharide ameliorates vascular endothelial dysfunction by stimulating macrophage M2 polarization via potentiating Nrf2/HO-1 signaling pathway. *Phytomed: Int J Phytother Phytopharmacology*. (2023) 112:154667. doi: 10.1016/j.phymed.2023.154667

39. Dong J, Lu J, Cen Z, Tang Q, Li Y, Qin L, et al. Cardiac macrophages undergo dynamic changes after coxsackievirus B3 infection and promote the progression of myocarditis. *J Med Virol*. (2023) 95:e29004. doi: 10.1002/jmv.29004

40. Liu L, Zhang Y, Zheng X, Jin L, Xiang N, Zhang M, et al. Eosinophils attenuate arthritis by inducing M2 macrophage polarization via inhibiting the IκB/P38 MAPK signaling pathway. *Biochem Biophys Res Commun*. (2019) 508:894–901. doi: 10.1016/j.bbrc.2018.12.010

41. Zhou F, Mei J, Han X, Li H, Yang S, Wang M, et al. Kinsenoside attenuates osteoarthritis by repolarizing macrophages through inactivating NF-κB/MAPK signaling and protecting chondrocytes. *Acta Pharm Sin B*. (2019) 9:973–85. doi: 10.1016/j.apsb.2019.01.015

42. Seshacharyulu P, Pandey P, Datta K, Batra SK. Phosphatase: PP2A structural importance, regulation and its aberrant expression in cancer. *Cancer Letters*. (2013) 335:9–18. doi: 10.1016/j.canlet.2013.02.036

43. Tschöpe C, Ammirati E, Bozkurt B, Caforio ALP, Cooper LT, Felix SB, et al. Myocarditis and inflammatory cardiomyopathy: current evidence and future directions. *Nat Rev Cardiol*. (2021) 18:169–93. doi: 10.1038/s41569-020-00435-x

44. Caforio ALP, Adler Y, Agostini C, Allanore Y, Anastasakis A, Arad M, et al. Diagnosis and management of myocardial involvement in systemic immune-mediated diseases: a position statement of the European Society of Cardiology Working Group on Myocardial and Pericardial Disease. *Eur Heart J*. (2017) 38:2649–62. doi: 10.1093/eurheartj/ehx321

45. Trachtenberg BH, Hare JM. Inflammatory cardiomyopathic syndromes. *Circ Res*. (2017) 121:803–18. doi: 10.1161/CIRCRESAHA.117.310221

46. McCarthy RE3rd, Boehmer JP, Hruban RH, Hutchins GM, Kasper EK, Hare JM, et al. Long-term outcome of fulminant myocarditis as compared with acute (nonfulminant) myocarditis. *New Engl J Med*. (2000) 342:690–5. doi: 10.1056/NEJM200003093421003

47. Pollack A, Kontorovich AR, Fuster V, Dec GW. Viral myocarditis–diagnosis, treatment options, and current controversies. *Nat Rev Cardiol*. (2015) 12:670–80. doi: 10.1038/nrcardio.2015.108

48. Zhang Y, Zhu L, Li X, Ge C, Pei W, Zhang M, et al. M2 macrophage exosome-derived lncRNA AK083884 protects mice from CVB3-induced viral myocarditis through regulating PKM2/HIF-1α axis mediated metabolic reprogramming of macrophages. *Redox Biol*. (2024) 69:103016. doi: 10.1016/j.redox.2023.103016

49. Almeida Paiva R, Martins-Marques T, Jesus K, Ribeiro-Rodrigues T, Zuzarte M, Silva A, et al. Ischaemia alters the effects of cardiomyocyte-derived extracellular vesicles on macrophage activation. *J Cell Mol Med*. (2019) 23:1137–51. doi: 10.1111/jcmm.14014

50. Xiong T, Zheng X, Zhang K, Wu H, Dong Y, Zhou F, et al. Ganluyin ameliorates DSS-induced ulcerative colitis by inhibiting the enteric-origin LPS/TLR4/NF-κB pathway. *J Ethnopharmacol*. (2022) 289:115001. doi: 10.1016/j.jep.2022.115001

51. Han-Wei Y, Ying-Da F, Na T, Feng-Chuan C, Ying-Feng L, Wei C, et al. Viral myocarditis: From molecular mechanisms to therapeutic prospects. (2024) 982:176935. doi: 10.1016/j.ejphar.2024.176935

52. Satoh M, Nakamura M, Akatsu T, Shimoda Y, Segawa I, Hiramori K. Toll-like receptor 4 is expressed with enteroviral replication in myocardium from patients with dilated cardiomyopathy. *Lab Investig J Tech Methods Pathol*. (2004) 84:173–81. doi: 10.1038/labinvest.3700031

53. Bao J, Sun T, Yue Y, Xiong S. Macrophage NLRP3 inflammasome activated by CVB3 capsid proteins contributes to the development of viral myocarditis. *Mol Immunol*. (2019) 114:41–8. doi: 10.1016/j.molimm.2019.07.012

54. Lee W, Lee S, Choi J, Park JH, Kim KM, Jee JG, et al. Antithrombotic properties of JJ1, a potent and novel thrombin inhibitor. *Sci Rep*. (2017) 7:14862. doi: 10.1038/s41598-017-13868-1

55. Chen C, Cai S, Wu M, Wang R, Liu M, Cao G, et al. Role of cardiomyocyte-derived exosomal microRNA-146a-5p in macrophage polarization and activation. *Dis Markers*. (2022) 2022:2948578. doi: 10.1155/2022/2948578

56. Loyer X, Zlatanova I, Devue C, Yin M, Howangyin KY, Klaihmon P, et al. Intra-cardiac release of extracellular vesicles shapes inflammation following myocardial infarction. *Circ Res*. (2018) 123:100–6. doi: 10.1161/CIRCRESAHA.117.311326